Studies of extreme-ultraviolet emission from Rydberg series of H_2 by electron impact

J. M. Ajello
Jet Propulsion Laboratory, California Institute of Technology, Pasadena, California 91109

D. Shemansky
Center for Space Sciences, University of Southern California, Tucson, Arizona 85713

T. L. Kwok and Y. L. Yung
Division of Geological and Planetary Sciences, California Institute of Technology, Pasadena, California 91125

(Received 19 May 1983)

Electron excitation cross sections have been measured for the following two Rydberg series of H_2: $^1\Sigma_u^+$ $1s\sigma np\sigma$ (B, B', and B'', states with principal quantum numbers $n=2$, 3, and 4, respectively) and $^1\Pi_u$ $1s\sigma np\pi$ (C, D, and D' states with principal quantum numbers $n=2$, 3, and 4, respectively) over the energy range from threshold to 350 eV. The cross sections for these six states account for all (>99%) of the vacuum-ultraviolet emission (78–170 nm) of the singlet states of H_2. The estimated total direct-excitation cross sections for these six states at 100 eV in decreasing value are $(4.02\pm0.60)\times10^{-17}$ cm^2 for $B\,^1\Sigma_u^+$ $(3.86\pm0.60)\times10^{-17}$ cm^2 for $C\,^1\Pi_u$, $(0.76\pm0.11)\times10^{-17}$ cm^2 for $D\,^1\Pi_u$, $(0.76\pm0.11)\times10^{-17}$ cm^2 for $B'\,^1\Sigma_u^+$, $(0.30\pm0.06)\times10^{-17}$ cm^2 for $D'\,^1\Pi_u$, and $(0.23\pm0.05)\times10^{-17}$ cm^2 for $B''\,^1\Sigma_u^+$ and, additionally, $(0.43\pm0.10)\times10^{-17}$ cm^2 for $E,F\,^1\Sigma_g^+$ which populates the $B\,^1\Sigma_u^+$ state through radiative cascade transitions. We estimate the predissociation (autoionization is weak) and emission yields of the vibrational levels of the D, D', and B'' states whose band systems exhibit strong "breaking off in emission" for wavelengths below 85 nm. Furthermore, we report the first direct measurement of the dissociative excitation cross section for production of Lyman-β of $(8.9\pm3.0)\times10^{-19}$ cm^2 at 100 eV. In particular, it is shown that the high-lying Rydberg states ($n=3$ and 4) make a substantial contribution to the observed emission below 110 nm while above 110 nm the Lyman bands ($B\,^1\Sigma_u^+\rightarrow X\,^1\Sigma_g^+$) and Werner bands ($C\,^1\Pi_u\rightarrow X\,^1\Sigma_g^+$), the first members of the Rydberg series, dominate the spectrum. As a result of these measurements and spectroscopic models the ultraviolet (UV) spectrum from H_2 by electron impact can serve as an intensity calibration standard from 80 to 170 nm.

INTRODUCTION

The ultraviolet absorption spectrum of H_2 has been known for 50 years to contain strong contributions from the $np\sigma$ and $np\pi$ Rydberg series.[1] On the other hand, we have only recently realized the significance of the higher Rydberg states, $n\geq3$, to the emission spectrum.[2,3] Work at this laboratory using an electron-beam technique and the work of Meudon Observatory with a discharge lamp technique[4] has demonstrated that the higher states must be included in modeling processes in order to account for the emission spectrum of H_2 in the extreme ultraviolet (euv).

We have recently discussed the results of emission cross-section measurements of the H_2 Lyman ($B\,^1\Sigma_u^+-X\,^1\Sigma_g^+$) and Werner ($C\,^1\Pi_u-X\,^1\Sigma_g^+$) systems in the far-ultraviolet (fuv) region from 120 to 170 nm.[5] In this paper we make a correction to the earlier work and extend the wavelength range of our investigation downward to include the euv region (70–120 nm), a region that contains the bulk of the Werner bands and all of the emissions generated from the next two members of each of these Rydberg series, $n=3,4$. In particular, the band systems[6] for these next members are $B'\,^1\Sigma_u^+\rightarrow X\,^1\Sigma_g^+$, $B''\,^1\Sigma_u^+\rightarrow X\,^1\Sigma_g^+$, $D\,^1\Pi_u\rightarrow X\,^1\Sigma_g^+$, and $D'\,^1\Pi_u\rightarrow X\,^1\Sigma_g^+$. Higher-lying Rydberg states ($n\geq5$) have been shown to contribute very few[4] emission features in the laboratory spectra of Meudon Observatory, and this absence is due mainly to autoionization to which must be added a small amount of predissociation.[7,8]

It is quite timely to investigate the vacuum-ultraviolet (vuv) emission spectrum of H_2, since molecular excitation by electron impact is the dominant emission process in the atmospheres of the outer planets[9] and since a wealth of uv emission data from these objects has been acquired from both planetary and earthbound spectrometers.[9,10]

In particular, the planetary data found most relevant to the euv results to be presented here are the Voyager uv spectrometer observations of Jupiter and Saturn.[9] An application of the results derived in this study has already been presented in the recent work of Shemansky and Ajello[2] which clearly showed that the Voyager uv observations could only be modeled by including emission from the $n=2,3,4$ Rydberg states of H_2.

Although H_2 is the simplest molecule from a structural point of view its uv spectrum is quite complex due to the relatively large separation of equilibrium internuclear distances[6] which cause extensive overlap of bands with comparable intensities. This is one of the fundamental reasons along with the difficulty of euv optical calibration tech-

niques that the analysis of the H_2 emission spectrum by electron impact has not been previously fully accomplished in the short-wavelength region. Nevertheless, a laboratory set of cross sections is important for verifying the accuracy of theoretical calculations. A review of the available experimental and theoretical cross-section data for the B and C states is given in Ajello *et al.*[5] Only a few authors have calculations for the other four states: Arrighini *et al.*[11] (B',B'',D,D') and Mu-Tao *et al.*[12] (B'). Additionally, there are no experimental absolute cross-section data for these four states. Shemansky and Ajello[2] have published semiempirical cross-section data making use of optical oscillator strengths.[13,14]

For the above reasons we have undertaken the task of determining emission cross sections by electron impact from 0 to 350 eV for the truncated Rydberg series $^1\Sigma_u^+$ $np\sigma$, $n=2,3,4$ and $^1\Pi_u$ $np\pi$, $n=2,3,4$. The method consists of measuring the calibrated emission spectrum of H_2 from 78 to 170 nm at a low resolution of 0.5 nm at an energy of 100 eV and fitting the laboratory spectrum with a synthetic spectrum of the same resolution. A graphical fitting technique has been applied to model the data. A similar fitting technique has been discussed previously in our analysis[5] of the fuv spectrum of H_2. The spectroscopic data used in the modeling have been discussed by Shemansky and Ajello.[2] Fitting a model to the data appears to provide a powerful tool for unfolding the complicated spectrum of H_2. The accuracy of the technique is limited by the absolute calibration of the optical system for strong band systems and, additionally for weak band systems, the degree to which they can be isolated from other band systems, at least over small spectral ranges. Certainly by "counting all the photons" from each of the vuv band systems of H_2 from 78 to 170 nm we are not making any assumptions about the cross section for the total band system as one must do if only isolated individual rotational lines or vibrational bands are used in the determination of total electron cross sections. For example, see Ajello *et al.*[5] for a discussion of the analysis of the data of Stone and Zipf.[15] Reanalysis of the fuv spectrum of our last work in the 110.0—170.0-nm region combined with the analysis of the present euv work (70.0—130.0 nm) makes it possible to obtain an accurate model fit to the cross sections of the six Rydberg states. We find that the analysis on the expanded spectrum yields cross-section values for the Lyman and Werner systems larger by $\sim 25\%$ than the earlier work by Ajello *et al.*[5]

The difference in these two results is caused basically by an error in the earlier work in the theoretical calculation of the relative production terms of the E,F-B transition in populating the B-state vibrational levels, rather than uncertainty in data analysis. Once this error is removed the original analytical method of Ref. 5 yields the same results as those presented here. These matters are discussed in detail in the body of the paper.

Predissociation has an important effect on a number of transitions in the higher series ($n=3,4$) states and contributes measurably to the total dissociation rate of H_2. Autoionization in the $n=3,4$ states is of lesser importance.[7,16] It is well known from high-resolution absorption studies[17] that predissociation begins at about 14.68 eV photon energy for the P and R branches of each of the B'', D, and D' states (the B' state is not predissociated although we report a population that is depressed by 25% in $v'=4$) due to various interactions (homogeneous, heterogeneous, and accidental predissociations, respectively) with the continuum of the B' state. These predissociative interactions range from fast for the $D\,^1\Pi_u^+$ state ($\tau_{\text{diss}} \sim 10^{-12}$ s) to slow for the $D'\,^1\Pi_u^+$ state ($\tau_{\text{diss}} \sim 10^{-8}$ s) to essentially zero (τ_{diss} large) for the $D\,^1\Pi_u^-$ and $D'\,^1\Pi_u^-$ states.[7] The predissociation quantum yield is unity only for fast predissociation. Thus the emission measurements provide for the first time direct measures of the emission and predissociation yields for each vibrational level. A summary of important recent work in the study of the predissociation of H_2 is given in the bibliographies of Refs. 8 and 16.

Finally, another interesting facet of this experiment is the determination of the H Lyman-β (Ly-β) cross section for dissociative excitation. This measurement, to our knowledge, has not been reported in the literature. Since Ly-β lies among several strong Werner Bands, careful analysis of the spectral intensities are required.

INSTRUMENTATION AND CALIBRATION

The instrumentation used in this experiment has been described in a previous paper.[18] In brief, the instrument consists of an electron impact emission chamber in tandem with a uv spectrometer. A magnetically collimated beam of electrons of variable energy (1 eV to 1 keV) is crossed with a beam of gas formed by a capillary which results in adjustable background gas pressures from 1×10^{-7} to 2×10^{-5} Torr. Inelastic electron-molecule collisions lead to emission of photons which are observed at right angles with respect to the electron beam axis. The uv spectrometer is an $f/4.5$ 20-cm-focal-length McPherson 234 Monochromator with an osmium-coated holographic grating. The detector is a Galileo Optics Channeltron (CEM), Model No. 4503.

In order to perform an optical calibration for the H_2 euv emissions to be presented here it is necessary to make a measurement of the relative wavelength sensitivity of the spectrometer and detector over the range from 78 to 125 nm. However, the relative calibration to be described here spans the entire range of the spectrometer and detector from 50 to 130 nm. Following the determination of the relative calibration, the absolute response of the optical system is determined from the modeled Ly-α (121.6 nm) line when H_2 is excited by 100-eV electrons. The experiments of Mumma and Zipf[19] together with those referenced in their publication have determined this cross section to be 1.18×10^{-17} cm^2.

The relative wavelength calibration of the spectrometer was determined by three separate procedures, which overlapped each other in wavelength. This precaution serves to check for consistency. These procedures were as follows.

(1) Optical calibration by a double monochromator arrangement from 50 to 120 nm.

(2) Molecular branching ratio technique for C state of H_2 from $H_2 + e(100\text{ eV})$ spectra in which we made use of

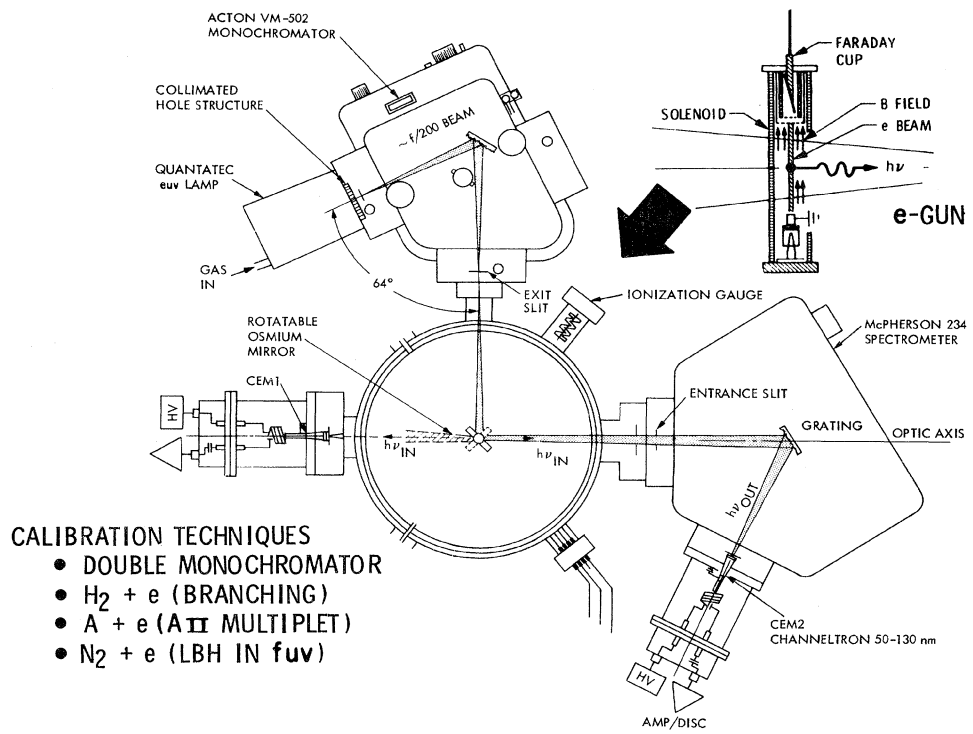

FIG. 1. Double monochromator calibration arrangement. Acton VM 502 monochromator acted as a monochromatic source for the McPherson 234 spectrometer as shown. Shaded areas representing the beam and the entrance slit are greatly exaggerated for clarity. In practice the beam actually underfills the entrance slit of the McPherson spectrometer. Electron gun which ordinarily occupies the center of the chamber is shown as an insert.

the transition probabilities of Allison and Dalgarno[20] over the wavelength range 105 to 130 nm (see Discussion section for further information on this technique).

(3) Relative experimental emission cross section observations of *A* II multiplets between 70 and 100 nm from *A* + *e*(200 eV) spectra at the "magic angle" which were compared to calibrated results of Mentall and Morgan.[21]

The experimental set up for the double monochromator measurement is shown in Fig. 1. In this arrangement the Acton VM-502 spectrometer could serve as a monochromatic source for either the McPherson 234 or CEM1; the latter was used to monitor the monochromatic intensity input to the McPherson 234. The windowless, collimated hole structure lamp, recently developed by Quantatec Corporation, required no water cooling and provided sufficient line intensity at 0.5-nm resolution for the euv calibration. The narrow (2 mm×0.2 mm) calibration beam at the position of the osmium mirror closely simulated the size and location of the H_2 collision region which was at the center of the 32.5-cm-diameter collision chamber. This arrangement ensured the same part of the grating was calibrated as used in the experiment. The sensitivity of the CEM was based on the known sodium salicylate fluorescence efficiency.[22] The resultant inverse sensitivity of spectrometer and detector from this optical calibration procedure is shown in Fig. 2.

Equally important calibration information was obtained by the other two procedures outlined previously. The consistency of the three calibration procedures is demonstrat-

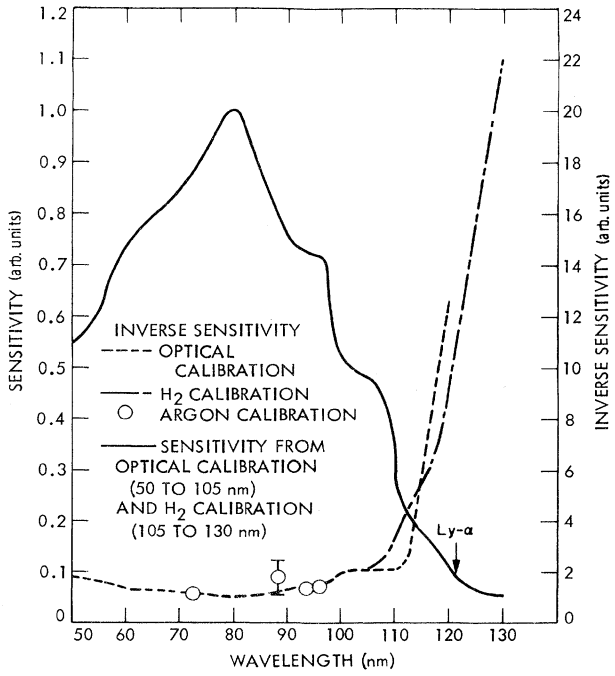

FIG. 2. Instrumental sensitivity and inverse sensitivity are shown as a function of wavelength as determined by three separate calibration techniques. The *A* II multiplets are at 72.5 92.0, and 93.2 nm. The two *A* I multiplets near 87 nm lead to a calibration value that is uncertain by 30% (error bars indicated) due to radiation trapping effects.

ed in Fig. 2 which also shows the inverse sensitivity for each of the three techniques. The resultant sensitivity is also shown. The calibration sensitivity is given by the combined optical calibration and $A+e$(200 eV) techniques, which agree to 15% where the techniques overlap from 50 to 105 nm, and by the H_2 branching ratio procedure from 105 to 130 nm. In the longer-wavelength region the signal-to-noise ratio was larger for the H_2 calibration technique than for the optical calibration. Additionally, polarization effects for the H_2 calibration are small.[5,23] On the other hand, for the optical calibration method polarization effects need to be considered when using a Seya mount-type spectrometer (angle of incidence near 32°) as a source. We have corrected our relative optical calibration sensitivity values for the effect of using partially polarized light in the double monochromator calibration. Two physical factors in an optical measurement lead to produce polarized light: (1) off-normal reflection and (2) diffraction effects at the grooves when $\lambda/d \geq 0.5$, where d is groove spacing and λ is wavelength. We can eliminate the second effect, since for a 1200-line/mm grating in the euv $\lambda/d \cong 0.1$. We will concentrate our discussion on the first effect. The Acton monochromator (angle of incidence near 32°) and osmium mirror (angle of incidence 45°), which act in tandem as a source for the McPherson 234, irradiate the McPherson 234 with almost a factor of 4 more radiation polarized perpendicular to the plane of incidence than parallel to it. We have used Fresnel's equations to calculate the polarization by reflection. This approach has been described in detail by Samson,[22] who additionally has verified experimentally the validity of these equations in the euv. We have substituted in Fresnel's equations the complex index of reflection for polycrystalline osmium[24] in order to calculate the parallel and perpendicular reflectances as a function of wavelength for the geometry of Fig. 1. A straightforward geometric ray tracing allows an analytical derivation of the correction factor to the measured relative grating efficiency for unpolarized light. This correction factor to the *relative* grating efficiency is less than 10%. Qualitatively this is true because the parallel and perpendicular components of reflectance have similar wavelength dependences (50—130 nm). On the other hand, if the *absolute* grating efficiency had been determined by this method, the correction factor would be larger. In this experiment the absolute system sensitivity (efficiency for the grating for unpolarized light times CEM quantum efficiency) was determined by the Ly-α calibration at 100-eV electron impact energy. In this regard the angular distribution of Ly-α photons was measured at 100-eV impact energy for emission angles between the magic angle and 90°. It was found that the variation was less than 5%.[23]

The overall sensitivity characteristic of the instrument at long wavelengths shown in Fig. 2 is determined by the rapid decrease in sensitivity of the channeltron. The short-wavelength response is determined primarily by the decrease in efficiency with wavelength of the grating which is optimized for 110 nm. If we fix the Ly-α cross section at exactly 1.18×10^{-17} cm^2 at 100 eV then the absolute accuracy of the cross sections presented here is estimated to be 15% for the B, C, B', and D states; 20% for the B'' and D' states, 25% for the E,F cascade contribution to the B state and 33% for Ly-β. The relative uncertainty with wavelength is estimated to be 15% in both the euv and fuv spectral regions. The total uncertainty reflects also the sensitivity of the cross-section parameter in the model to the data.

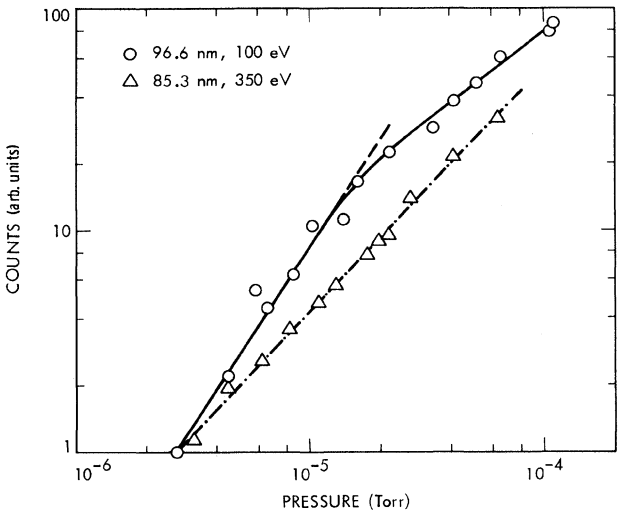

FIG. 3. Pressure linearity tests for two spectral features indicated in Table I. These features are predominantly the (2,0) Werner band at 96.6 nm and the D(2,0) band at 85.3 nm.

In addition, we have obtained spectra of H_2 in the range of optical depths for self-absorption where the signal is linear with pressure. The results of a linearity test at two wavelengths are shown in Fig. 3. The 96.6-nm feature is dominated by the (2,0) Werner band and the feature at 85.3 nm is dominated by the D-X (2,0) band. The results shown in Fig. 3 indicate absorption is important for the Werner bands with $v''=0$ at pressures of 10^{-5} Torr or greater. The nonlinear pressure effects occur for foreground column densities greater than 2×10^{13} cm^{-2}. The experiments reported here were conducted over a range of pressures from 5×10^{-6} to 2×10^{-5} Torr and small effects of self-absorption for the ($v''=0$) v' progression are easily taken into account by the model.

EXPERIMENTAL RESULTS

We show in Fig. 4 an experimental spectrum for the wavelength range 70 to 170 nm resulting from 100-eV electron impact excitation of H_2. The region labeled fuv was the subject of our previous work on H_2; and the region labeled euv is the subject of our present analysis. We have combined both these calibrated spectra obtained at slightly different resolutions in order to provide an experimental spectrum showing all the vuv bands from singlet states of H_2. The $a\,^3\Sigma_g^+ \rightarrow b\,^3\Sigma_u^+$ continuum transition does not contribute significantly to the fuv laboratory spectrum at 100 eV. Measureable amounts of a-b radiation are indicated at low ($\sim$20 eV) energies below 170 nm.

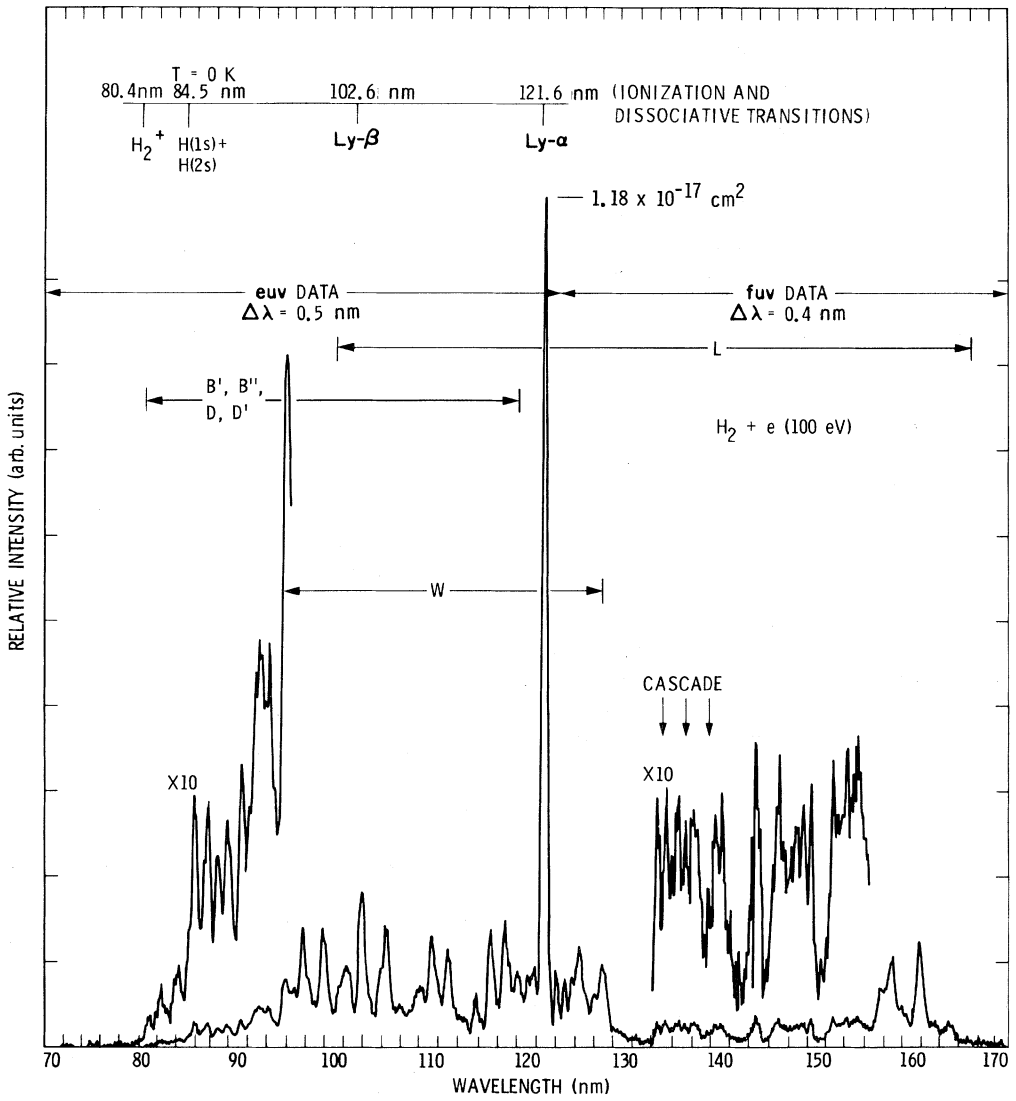

FIG. 4. Calibrated laboratory spectrum of H_2 at 100-eV electron impact energy. Arrows indicate wavelength regions of strong cascading emission. euv data were measured in this work and the fuv data were analyzed in a previous paper.[5] Spectra were joined at about 123 nm. Wavelength resolution was 0.5 nm for the euv data and was 0.4 nm for the fuv data. Background pressures in the chamber were 8×10^{-6} Torr for the euv data and 2×10^{-5} Torr for the fuv data.

In this section we examine the 100-eV spectrum and provide model fits for each region in order to determine the cross sections of each member of the Rydberg series. The important features of this 100-eV spectrum are the following.

(1) The strong vibrational development of the upper states in the excitation process produces a complex spectrum of overlapped bands from the six electronic systems. The analysis of the observations consequently requires comparison with detailed model calculations. In discharge lamps this spectrum[22] is often referred to as the hydrogen many-line spectrum, and indeed the model calculations in the present work involve the order of 30 000 fine-structure transitions in the 78—170-nm region.

(2) The spectral threshold of the bands is 78 nm, ~0.47 eV above the ionization energy.

(3) Significant "breaking off of the bands" caused by predissociation begins at 85 nm and extends to shorter wavelengths.

(4) The emission below 90 nm is dominated by the $n=3,4$ series transitions; the Werner and Lyman bands lie mainly above 90 nm.

(5) The feature near 102.5 nm, dominated by the (1,1) 102.9-nm and (3,2) 102.5-nm Werner bands, is enhanced over the model calculation and attributed to the Ly-β transition.

(6) The $E,F\,^1\Sigma_g^+ \rightarrow B\,^1\Pi_u^+$ transition has a measurable effect on the emission distribution of the Lyman B-X system, as discussed by Ref. 5. The E,F relative contribution arises sharply at low energies and is an important diagnos-

tic indicator of electron energy.

(7) The strength of the Lyman continuum transitions near 160 nm has been previously discussed.[20]

Due to the complexity of the spectrum indicated in item (1) we have identified in Table I the 49 spectral features observed in the euv region of the spectrum at 0.5-nm resolution. This table gives an indication of the number of bands under each observed feature and the theoretical relative intensities at the peak for 100-eV electron-impact energy.

Although the band systems are heavily blended it is possible to obtain a unique theoretical model since each system has regions of dominance in the spectrum. The best fit to the laboratory spectrum in the euv region is shown in Fig. 5(a) and the best fit to the fuv region is shown in Fig. 5(b). The tabulated excitation cross-section data for all six electronic transitions, including the cascade contribution from the E,F state to the B state are shown in Table II. Note the rapid falling off in cross section with principal quantum number for each Rydberg series. In addition, Table II shows our results in comparison to other estimates. These estimates are from the work of Shemansky and Ajello,[2] Ajello *et al.*,[5] Mu-Tao *et al.*,[12] Fliflet and McKoy,[25] Arrighini *et al.*,[11] Gerhardt,[26] and Stone and Zipf.[18] A more complete set of theoretical and experimental estimates for the B and C states is given in our previous work.[5] The B-state cross section is most accurately determined in the fuv region. The C-state cross section determined from both the fuv- and euv-region spectra agree, in the analysis presented here, to $\sim 15\%$. The model, on the other hand, is not sensitive to the cross section of the B'' state. The B'' state is completely predissociated for $v' > 0$. For this cross section on the basis of the model fit it is sufficient to use the

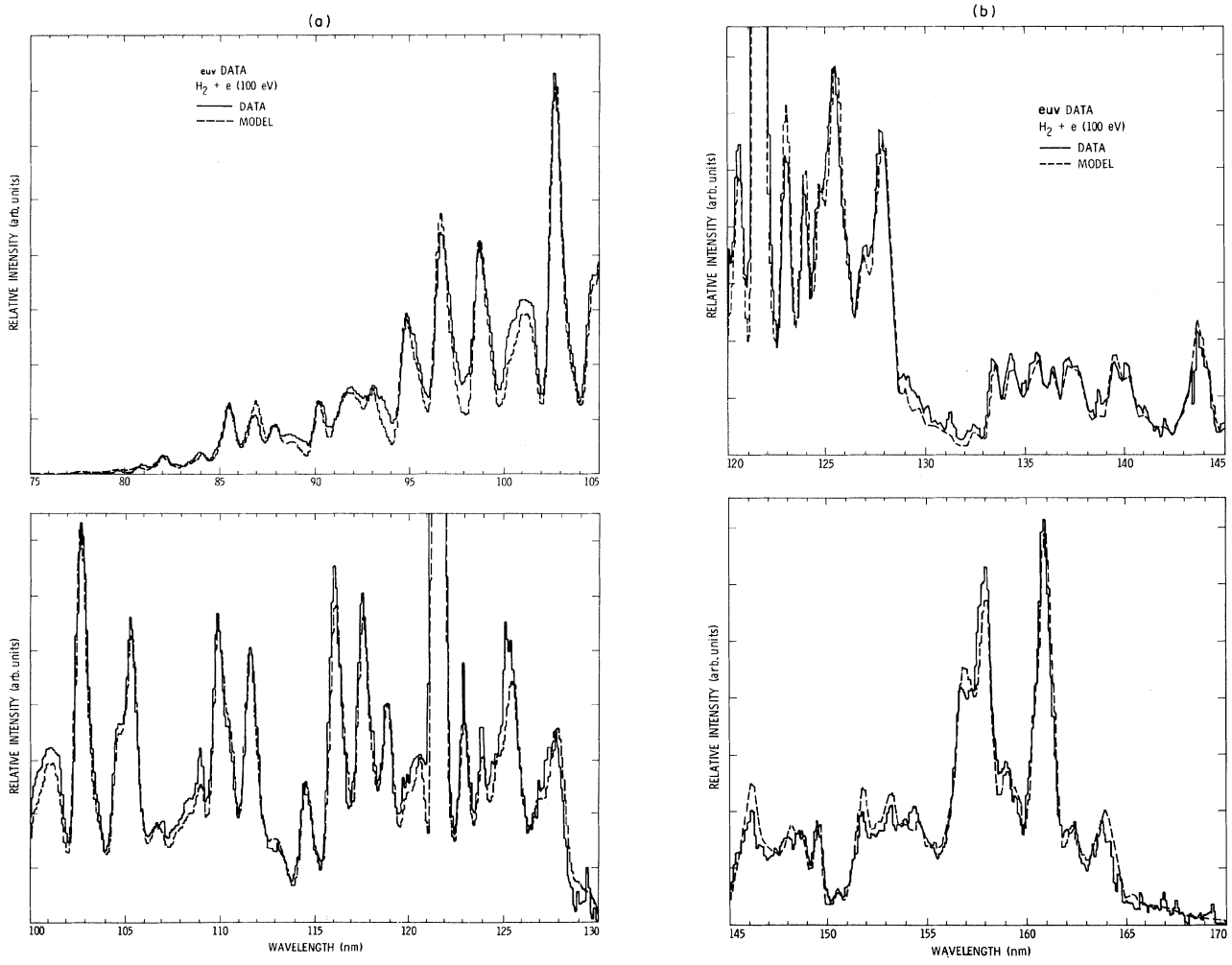

FIG. 5. Best model fit for the euv region to a laboratory spectrum observed at 100-eV impact energy and a gas background pressure of 2×10^{-5} Torr. References for the modeling parameters for the molecular band systems are given in Shemansky and Ajello (Ref. 2). Magnitude of the total cross section for each electronic transition used in the model is given in Table II for the molecular transitions and in Table IV for the atomic transitions. This model includes predissociation and self-absorption effects for the Werner bands as described in the text. Excitation cross sections deduced for this spectrum are identical to the results obtained for the lower-pressure euv spectrum of Fig. 4. Solid line indicates the data and the dashed line indicates the model. (b) Best model fit for the fuv region to the laboratory spectrum of Fig. 4 at a pressure of 2×10^{-5} Torr.

TABLE I. All euv emission features of H_2 at 0.5-nm resolution and 100 eV electron-impact energy.

Feature no.	Observed wavelength (nm)	*B*	*B'*	*B''*	*C*	*D*	*D'*	Theoretical relative intensity at peak
1	77.8						(6,0),(9,1),(13,2),(14,2),(15,2)	3.0
2	78.4						(5,0),(8,1),(12,2)	2.0
3	79.3						(4,0),(7,1),(10,2),(15,3)	4.0
4	80.9						(3,0),(8,2),(12,3)	7.0
5	82.0					(5.0)	(2,0),(7,2),(10,3),(14,4),(15,4)	20.0
6	83.8			(4,1)		(3,0)		22.0
7	85.3		(5,0),(6,0)			(2,0)	(0,0),(6,3)	74.0
8	86.8			(4,2)		(1,0)	(1,1)	81.0
9	87.7		(2,0)	(1,11)		(1,0),(7,3)	(2,2)	53.0
10	88.9	(23,0)	(1,0),(4,1)			(4,2)		35.0
11	90.2	(27,1)		(1,2),(3,3)		(1,1),(3,2),(5,3)		80.0
12	92.3	(17,0),(23,1) (31,2)	(1,1),(4,2)		(7,1)		(1,3)	84.0
13	93.0	(18,0),(22,1) (23,1)	(3,2)		(4,0),(6,2),(7,1)			97.0
14	94.8	(14,0),(19,1)	(2,3)		(3,0),(8,2),(12,3)	(2,3)	(0,3)	185.0
15	96.6	(12,0),(18,1)	(3,3)	(1,4)	(2,0),(7,2),(10,3)	(1,3)	(2,5)	315.0
16	98.7	(10,0),(14,1)	(2,3)		(1,0),(3,1),(11,4)		(1,5)	289.0
17	100.8	(8,0),(13,1)			(0,0),(2,1),(4,2), (6,3),(12,5)	(4,6)	(11,14),(4,8)	
18	101.4	(7,0),(11,1)	(2,4),(0,3)		(0,0),(2,1),(6,3), (8,4),(11,5)	(2,5)	(5,9),(1,6)	183.0
19	102.7	(11,1),(23,4)	(4,5)	(1,6)	(1,1),(3,2),(5,3), (7,4),(10,5)	(3,6),(9,10)	(3,8)	433.0[a]
20	105.3	(4,0),(25,5)			(2,2),(0,1),(4,3), (6,4),(8,5),(11,6)	(2,6),(3,7)		315.0
21	109.0	(1,0),(4,1),(5,1), (11,3)			(7,6),(0,2),(12,8), (13,8)			150.0
22	111.7	(6,2)			(6,6),(3,4),(1,3)			323.0
23	114.6	(1,1),(4,2),(14,5), (18,6),(22,7)			(3,5),(0,3)			301.0
24	116.2	(0,1),(3,2),(13,5), (20,7),(24,8)			(4,6),(1,4)			349.0
25	117.5	(9,4),(12,5),(15,6), (19,7),(22,8)			(10,10),(5,7),(2,5), (6,3)			335.0
26	119.1	(11,5),(14,6),(17,7)			(9,10),(3,6),(0,4)			240.0
27	120.5	(4,3),(7,4)			(7,9),(4,7),(1,5)			180.0
28	121.6	(1,2)			(9,11),(5,8),(1,5)			
29	123.0	(0,2),(8,5),(11,6)			(11,14),(3,7)			219.0
30	123.9				(9,12),(4,8),(0,5)			183.0

TABLE I. (*Continued.*)

Feature no.	Observed wavelength (nm)	*B*	*B'*	*B''*	*C*	*D*	*D'*	Theoretical relative intensity at peak
31	125.4	(15,8),(18,9)			(5,9),(6,10),(7,11), (8,12),(9,13),(1,6)			264.0
32	127.7	(8,6),(16,0),(21,11)			(3,8),(4,9),(5,10),(7,12)			213.0
33	133.5	(5,6),(3,5),(0,4)						62.0
34	134.4	(7,7),(12,9)						62.0
35	135.7	(9,8),(4,6),(11,9), (15,11)						67.0
36	136.4	(15,11)						59.0
37	137.2	(14,11),(17,13)						60.0
38	139.5	(9,9),(11,10),(13,11), (0,5)						68.0
39	140.1	(7,8),(13,11),(14,12), (2,6)						56.0
40	143.6	(9,10),(7,9),(5,8), (3,7),(1,6)						98.0
41	146.1	(12,13),(6,9),(4,8), (2,7)						111.0
42	149.3	(8,11),(11,14),(7,10), (11,14)						73.0
43	151.6	(10,14),(10,7), (4,9),(2,8)						115.0
44	153.1	(5,10),(8,12),(9,13),						92.0
45	154.2	(9,14),(3,9)						79.0
46	156.6	(8,14),(4,10),(8,14)						184.0
47	157.8	(5,11),(6,12),(7,13), (2,0),(0,8)						229.0
48	160.6	(4,11),(1,9),(6,13), (1,0),(5,12)						277.0
49	163.7	(5,13),(3,11)						85.0

[a]Contains small contribution from H Ly-β.

TABLE II. Table of excitation and emission cross sections at 100 eV for H_2. Sources were as follows: *A*, this work; *B*, Shemansky and Ajello (Ref. 2); *C*, Ajello *et al.* (Ref. 5), *D*, Arrighini *et al.* (Ref. 11); *E*, Mu-Tao *et al.* (Ref. 12) and Fliflet and McKoy (Ref. 25); *F*, Gerhardt (Ref. 26); *G*, from Stone and Zipf (Ref. 15), see text.

			Q (10^{-17} cm^2)									
State	Threshold elec. Energy T_e (eV)	Symbol	Source A	B	C	D	E	F	G	Emission yield of elec. state (%)	Emission cross sections of elec. state	Prediss. cross section into H(2s) + H(1s)
$B\,^1\Sigma_u^+$ $2p\sigma$	Cascade 12.41	Q_A	0.43		0.85	0.43				100	0.43	
$B\,^1\Sigma_u^+$ $2p\sigma$	Direct 11.37	Q_B	4.02	3.53	2.7	3.32	3.9	4.3		100	4.02	
$C\,^1\Pi_u$ $2p\pi$	12.41	Q_C	3.86	3.08	3.1	3.48	3.1	4.8	4.6	100	3.86	
$B'\,^1\Sigma_u$ $3p\sigma$	13.84	$Q_{B'}$	0.76	0.63		0.67	0.35			100	0.76	
$D\,^1\Pi_u$ $3p\pi$	14.12	Q_D	0.76	0.78		0.91				70.2	0.53	0.23
$B''\,^1\Sigma_u^+$ $4p\sigma$	14.63	$Q_{B''}$	0.23[a]	0.19		0.27				3.3	0.01	0.22
$D'\,^1\Pi_u$ $4p\pi$	14.74	$Q_{D'}$	0.30	0.25		0.39				42.1	0.13	0.17
		Total	10.36								9.74	0.62

[a]Average of columns *B* and *D*.

theoretical value shown in Table II. The agreement between the experimental values and the theoretical values for all electronic states now appears to be within 20%, which can be considered quite good.

The excitation cross sections for the higher members ($n \geq 3$) of the Rydberg series are not equal to the emission cross sections. For this reason the branching ratio yields for emission and predissociation for the excitation cross sections are given in Table III for each vibrational level. A comparison of our predissociation and emission yields with the high-resolution work of Guyon *et al.*[8] is also given in Table III. In our case the yield represents an average of the unresolved $^1\Pi_u^+$ and $^1\Pi_u^-$ vibrational and rotational levels. However, the excitation and emission probabilities are known for the fine structure and a direct comparison can be made. Additionally, Guyon *et al.*[8] have shown (1) the predissociation yields of all the rotational levels of the $v=3-11$ levels of the $D\,^1\Pi_u^+$ state to be equal to unity; (2) the predissociation yields of the $v=1-7$ levels of the $D'\,^1\Pi_u^+$ state to vary slowly with rotational quantum number except for $v=5$ and to be equal to about $80\pm10\%$ for all vibrational levels; and (3) the predissociation yields of the $D\,^1\Pi_u^-$ and $D'\,^1\Pi_u^-$ states to be less than 5% and which we arbitrarily set equal to zero. Furthermore, the results of Dehmer and Chupka[7] indicate that for the vibrational levels of the *D* state with $v \geq 9$ and of the *D'* state with $v \geq 4$, autoionization is effective for both the + and − components. Above these critical values the emission yield is small. However, a weak emission is observed from the higher levels for energies above the ionization potential.

The high-resolution absorption linewidth results of Rothschild *et al.*[16] for the *B''* state indicate the predissociation yield is unity for $v>0$. With these background statements it is reasonable that our low-resolution results agree well with the average results for the high-resolution studies.

We further expand on Table III to obtain the total predissociation and emission yield for each electronic state. It is defined as

$$\eta^P = \sum_{v'} q_{v'0}\eta^P_{v'}$$

and (1)

$$\eta^E = \sum_{v'} q_{v'0}\eta^E_{v'}$$

for predissociation and emission, respectively. It is assumed here that excitation rates are proportional to the Franck-Condon factors for the transitions. For this calculation the Franck-Condon factors for the *D* and *B'* electronic states are taken from Spindler.[27] The Franck-Condon factors $q_{v'0}$ are shown in Table III. It is assumed the Franck-Condon factors for the *D* and *B'* states are identical to those of the *D'* and *B''* states, respectively, since the relevant internuclear distances are nearly identical.[6] The emission and predissociation cross sections calculated using Eq. (1) are shown in the last two columns of Table II. These results are based on the total predissociation and emission yields calculated in Table III from Refs. 8 and 10. By definition the emission cross section is the product of the emission yield and excitation cross section. Note that all other electronic states except for *D*, *D'*, *B''*, and possibly one level of *B'* have an emission yield of 100%.

Additionally, the branching ratio for vuv radiation to the ground state for these six electronic states is assumed to be unity. The *D* state has been observed to produce visible radiation via the transition[6] $D \rightarrow E$. However, since transition probabilities vary as the cube of the transition energy the branching ratio for the visible radiation is negligible and the emission cross section is to be associated entirely with the vuv transition. A similar argument applies to vibrational levels of the *B* state which lie above those of *E,F*.

TABLE III. Table of predissociation yields for low v'.

State	v'	$q_{v'0}$	Predissociation yield[a] $\eta_{v'}^{P}$ (%) Expt.	Est. from Refs. 8 and 16	Emission yield $\eta_{v'}^{E}$ (%) Expt.	Est. from Refs. 8 and 16
$D\,^1\Pi_u$	0	0.108	0	0	100	100
	1	0.182	0	0	100	100
	2	0.187	0	0	100	100
	3	0.154	55	50	45	50
	4	0.112	80	50	20	50
	5	0.077	60	50	40	50
	6	0.0514	80	50	20	50
	7	0.0338		50		50
	8	0.0223		50		50
	9	0.0148		100		0
	10	0.0101		100		0
$D'\,^1\Pi_u$	0	0.108	0	0	100	100
	1	0.182	50	40	50	60
	2	0.187	25	40	75	60
	3	0.154	60	40	40	60
	4	0.112	~90	100	~10	0
	5	0.077	~90	100	~10	0
	6	0.0514		100		0
	7	0.0338		100		0
	8	0.0233		100		0
	9	0.0148		100		0
	10	0.0101		100		0
$B''\,^1\Sigma_u^+$	0	0.0332	0	0	100	100
	1	0.0137	~90	100	~10	0
	2	0.102	~90	100	~10	0
	3	0.114	~90	100	~10	0
	4	0.105	~90	100	~10	0
	5	0.0674	~90	100	~10	0
	6	0.0155	~90	100	~10	0
	7	0.0021	~90	100	~10	0
	8	0.0052	~90	100	~10	0

[a]Includes a small amount of preionization yield for certain vibrational levels above a critical value as described in the text. The contribution of these v' by preionization is small compared to the total electronic predissociation.

The process of fitting the H_2 band models to the experimental data leaves a deficiency in the model calculation of the relative intensity of the feature near 102.5 nm. We have attributed this deficiency in the model to the dissociative excitation of H Ly-β. The inclusion of the appropriate H Ly-β signal required to fit the model to the data leads to an estimated cross section of 8.9×10^{-19} cm^2 at 100 eV for the process

$$e+H_2\rightarrow(Hnl)+H(nl)+e$$
$$\rightarrow 2H(1s)+h\nu(\text{Ly-}\alpha+\text{Ly-}\beta+\cdots+H\alpha+H\beta+\cdots)\,. \quad (2)$$

There is a similar process for production of a proton and excited hydrogen atom. The H Ly-β line arises in the $1s$-$3p$ transition and is therefore related directly to the production of Hα emission as one of the branches of reaction (2). There is a substantial background of experimental work on electron excited Balmer series radiation, which includes a number of measurements of the cross section for the production of Hα line emission and also its spectral line shape.[28–33] The spectral line shape has indicated that there are slow H fragments ($\epsilon\sim0.4$ eV) arising from dissociation of low-lying Rydberg states and fast H fragments from highly repulsive, doubly excited states ($\epsilon\sim10$ eV). There is generally very good agreement among the measurements of the Hα cross section, $\sigma(H\alpha)$, as shown in Table IV. If we accept the latest and possibly most carefully measured value,[32] $\sigma(H\alpha)=9.3\times10^{-19}$ cm^2 at 100 eV, the cross section for H Ly-β emission calculated from $\sigma(H\alpha)$ is $\sigma(\text{Ly-}\beta)=8.3\times10^{-19}$ cm^2, in excellent agreement with the direct measurement obtained in the present experiment. Details for these calculations and further dis-

TABLE IV. H_2 dissociative excitation cross sections at 100 eV. Sources were as follows: *J*, this work; *K*, Mumma and Zipf (Ref. 19) and references therein; *L*, Karolis and Harting (Ref. 32), see also Refs. 28 and 29; *M*, Moisewitsch and Smith (Ref. 34).

Transition	Threshold energy (eV)	Q (10^{-17} cm^2) Dissociative excitation of H_2 *J*	*K*	*L*	Direct excitation of H *M*
Ly-α $1s$-$2p$	14.67		1.18		6.8
Ly-β $1s$-$3p$	16.56	0.089			1.0
H $n=3\rightarrow2$ ($2s$-$3p$ + $2p$-$3d$ + $2p$-$3s$)	16.56	0.099		0.093	

cussion of the dissociative process are given in the following section. Table IV also shows for comparison purposes results for direct excitation of atomic H.[34]

We have measured the excitation function of the 85.3-nm feature which is primarily the $D(2,0)$ feature. The excitation function is shown in Fig. 6 and the tabular results in Table V. The shape agrees closely with that measured previously[5] for the Werner bands, particularly for $\epsilon > 30$ eV. In view of this result we assume that all high-lying Rydberg series for $n > 3$ have the same cross-sectional energy dependence for direct excitation as the first member of the Rydberg series. We plot in Fig. 7 the collection of absolute singlet excitation cross sections for the Rydberg-series transitions of H_2 studied in this work plotted as a function of energy from 0 to 300 eV. The cross sections are normalized to our values at 100 eV from Table II. In addition, we have added the Ly-α result of Mumma and Zipf[19] together with our result for Ly-β from Table IV. We have also measured the Ly-α excitation function and find the same relative energy dependence as Mumma and Zipf. We assume the Ly-β and Hα transitions have the same energy dependence for dissociative excitation and use the energy dependence as measured by Karolis and Harting.[32]

MODEL CALCULATIONS

Observations of the H_2 Rydberg systems with the resolution of the present experiment, 0.4 or 0.5 nm, could not be analyzed without the use of a model calculation including vibrational and rotational structure of the electron excited systems. The basic difficulty in attempting analysis in any other way is the heavy blending of bands from a broad range of upper-state vibrational levels. In this particular case the analysis has been eased considerably by the fact that the theoretical calculations of relative excitation

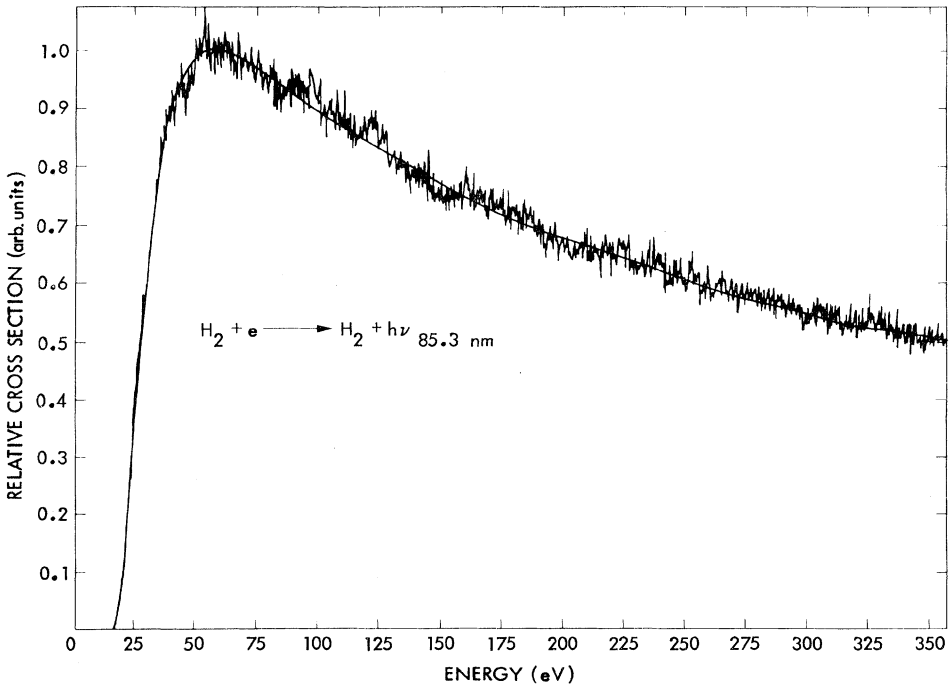

FIG. 6. Relative-emission cross section of the 85.3-nm spectral feature which is mostly the $D(2,0)$ transition.

TABLE V. Measured relative-emission cross section of H_2 for the excitation of the 85.3-nm vibrational feature.

Energy (eV)	Relative-emission cross section
20	~0.20
30	0.65
40	0.92
50	0.98
60	1.00
70	0.98
80	0.95
90	0.92
100	0.89
120	0.85
150	0.77
200	0.68
250	0.60
300	0.54
350	0.51

rates and transition probabilities fitted the observed spectra on the whole to a satisfactory degree of accuracy (better than 5%). In the short-wavelength region where predissociation alters the intensities of the bands of the higher Rydberg series the effects were obvious from wavelength correlations with the v'' progressions of the affected levels. Due to the importance of the model we feel it is necessary to describe the calculation of synthetic spectra here at least in a general way, and give detail where information is not supplied elsewhere in the literature.

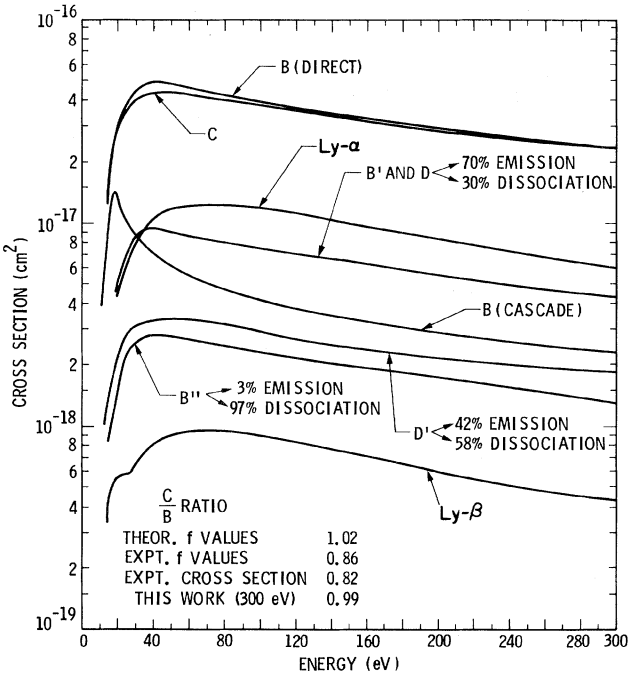

FIG. 7. A complete set of electronic cross sections for H_2 from electron impact based on Table II for the molecular transitions, Table IV for the Ly-β transition and on the work of Mumma and Zipf (Ref. 19) for Ly-α. Included in the graph are important C/B ratios as discussed in Ajello *et al.* (Ref. 5) in Table I and the discussion section of that reference. Note the B' and D cross-section curves are shown as the same.

In brief, the calculation that follows produces the model spectrum of discrete and continuum transitions in a H_2 gas excited by electrons. Ground-state molecules in vibrational and rotational thermal equilibrium are excited into the various electronic states according to the rate equations given below. The excitation transitions are calculated with probabilities determined according to the relevant overlap integrals for the rotational-vibrational-electronic structure (given in Table VI as normalized rates). The populations of the excited-state rotational and vibrational levels are then controlled by the balance of the upward-going excitations and the downward radiation and predissociative transitions, branched according to quantum selection rules and fine-structure transition probabilities. The intensities of the emission transitions are determined according to the relative downward transition rates.

The optically thin volume emission rate (I) of a band (v_j,v_i) of the electronic transition between upper state j and lower state i is calculated through an equation of the form [in $(\text{cm}^3\ \text{s}^1)^{-1}$]

$$I(j,i;v_j,v_i)=g(j;v_j;E_e)\frac{A(j,i;v_j,v_i)}{A(j,i;v_j)}K(v_j)\ , \tag{3}$$

where $A(j,i;v_j,v_i)$ is the spontaneous transition probability for the band,

$$A(j,i;v_j)=\sum_{v_i}A(j,i;v_j,v_i) \tag{4}$$

(in s^{-1}) is the total probability of radiative decay of vibrational level v_j, $K(v_j)$ is the fraction of the population undergoing radiative transition, and $g(j;v_j;E_e)$ is the excitation rate of the level v_j at electron energy E_e. The $A(j,i;v_j,v_i)$ values in the model calculations in every case were obtained from theoretical work referenced by Shemansky and Ajello.[2] The A values for the B-X and C-X transitions are given directly by Allison and Dalgarno[20] and Stephens and Dalgarno,[35] whereas those for the B'-X, B''-X, D-X, D'-X, and E,F-B transitions were calculated using Franck-Condon factors and oscillator strengths as described by Ref. 2. The electronic transition moments for the higher Rydberg states were assumed to be constant as a function of internuclear distance. The assumption of constancy of the electronic transition moment apparently is satisfactory for the B', B'', D, and D' states[13] but not for the E,F state. The E,F-B transition gives rise to emission in the near-infrared and infrared regions, but our concern here is with the contribution to the production of B-state molecules. Our treatment of the E,F-B component will be discussed in more detail below. With the exception of the E,F-B transition, the relative vibrational excitation rates for the states are strictly determined by the theoretical values at the Born limit,

$$g(j;v_j;\infty)\propto\nu^{-3}A(j,i;v_j,v_i)\ , \tag{5}$$

where ν is transition energy, $v_i=0$, and $i=X$.

Effectively, all of the ground-state molecules are in the $v=0$ level and (3) requires no summation terms over v_i.

The energy (E_e) dependencies of g for $j=C$, D,D' and $j=B,B',B''$ were taken from the shape functions of particular Werner and Lyman bands as described by Ref. 2 [see above discussion of the D-X (2,0) shape function, shown in Fig. 6]. Thus the collision strengths of the vibrational levels of a given state, written in terms of threshold units, all have the same shape. The threshold energies for the vibrational levels v_j are sufficiently separated for a given upper state to show moderate deviations from Eq. (5) even at $E_e=100$ eV and this is taken into account in the model calculations.

Rotational fine structure is taken into account by applying Hönl-London factors to the calculation of line strengths.[36] Rotational transition probabilities are then given by

$$A(j,i;v_j,v_i;J_j,J_i)=A(j,i;v_j,v_i)S_A(\Delta J)\ , \tag{6}$$

where $S_A(\Delta J)$ is the appropriate line-strength factor based on Hönl-London factors such that

$$A(j,i;v_j,v_i;J_j)=\sum_{J_i}A(j,i;v_j,v_i;J_j,J_i) \tag{7}$$

and

$$A(j,i;v_j,v_i)=A(j,i;v_j,v_i;J_j) \tag{8}$$

for any value of J_j. Summation over J_i in Eq. (7) is restricted to a single symmetric or antisymmetric level for Π states. Thus each upper-state fine-structure rotational level has the same lifetime as the characteristic value for the band transition (Eq. 8).

Fine-structure excitation rates g are calculated assuming that transition strengths are directly proportional to the optical absorption strengths (see Ref. 37 for absorption strengths),

$$g(j;v_j;J_j;E_e)=[g(j;v_j;E_e)/g(j;E_e)]\times S_B(\Delta J)F_eN(X;0;J_X)\sigma(i,j;E_e)\ , \tag{9}$$

where

$$N(X;0)=\sum_{J_X}N(X;0;J_X) \tag{10}$$

is the total ground-state population density, F_e and σ are the electron flux and total i,j cross section, $S_B(\Delta J)$ is the rotational absorption strength,

$$g(j;E_e)=\sum_{v_j}g(j;v_j;E_e)\ , \tag{11}$$

and

$$g(j;v_j;E_e)=\sum_{J_J}g(j;v_j;J_j;E_e)\ , \tag{12}$$

where symmetric and antisymmetric levels are maintained as separate systems according to nuclear spin statistical weights. The rotational population $N(X;0;J_X)$ of the ground state is assumed to be in a Maxwell-Boltzmann distribution.

Wavelengths are calculated using measured rotational, vibrational, and electronic energies of the states to an accuracy of $\sim 10^{-3}$ nm in unperturbed levels. Self-absorption effects in the H_2 foreground are included in the fine structure of the model calculations. The background pressure of 2×10^{-5} Torr in the observations shown in Fig. 5(a) corresponds to a H_2 foreground abundance of $\sim 3\times10^{13}$ cm^{-2}, a depth great enough to affect the intensities of the Werner band features between 95 and 100 nm. The fact that approximately this foreground abundance (3×10^{13} cm^{-2}) is required in the model to fit the data of Fig. 5(a) is a measure of the degree of accuracy to which the data can be fitted. Figure 4 shows a spectrum taken with a foreground H_2 abundance of $\sim 1\times10^{13}$ cm^{-2}, in which the effect of self-absorption is too small to measure.

As we have noted above, the excitation functions of the upper-state vibrational levels v_j, with the exception of the contribution of the E,F states, were fixed by the theoretical relative rates for a given J. The fitting of the model calculations to the observed spectra thus consisted of iterative combinations of the six j,i band systems, with each rotational line convolved with the triangular transmission function (ITF) of the instrument. An accurate measure of the width of the ITF is necessary for accurate cross section estimates and this parameter was measured by carefully fitting the model calculation to the shape of the HI 121.6-nm line. Each j,i band system in this model structure is therefore fixed in spectral shape by the theoretical relative excitation rates as discussed above, and cross sections were estimated by fitting the six systems, shown in Figs. 8 and 9 together to obtain an optimal fit to the data. The absolute cross sections are fixed relative to the measured cross section for dissociative excitation of the H Ly-α line[19] as noted above. In fitting the model calculations to the data we have found that with the exception of the E,F-B contribution, there is no justification for altering the theoretical relative $g(j;v_j)$ rates for a given state. This conclusion also holds for the relative rate of the B-X continuum transitions in the long-wavelength, 140—170-nm region.

DISCUSSION

The cross-section estimates of the H_2 Lyman and Werner systems are weighted heavily by the earlier mea-

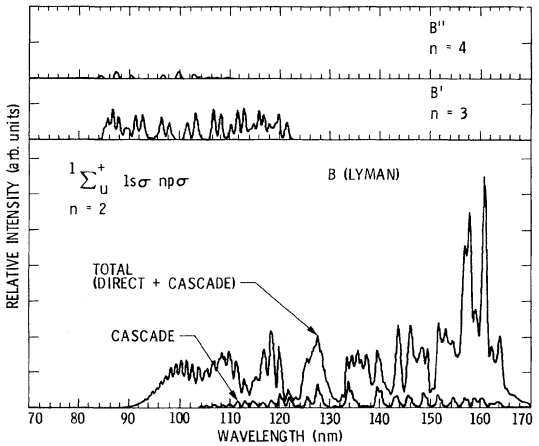

FIG. 8. A synthetic spectra of the $np\sigma$ Rydberg-series emission $n=2,3,4$ where the relative intensities are normalized to our experimental values at 100 eV.

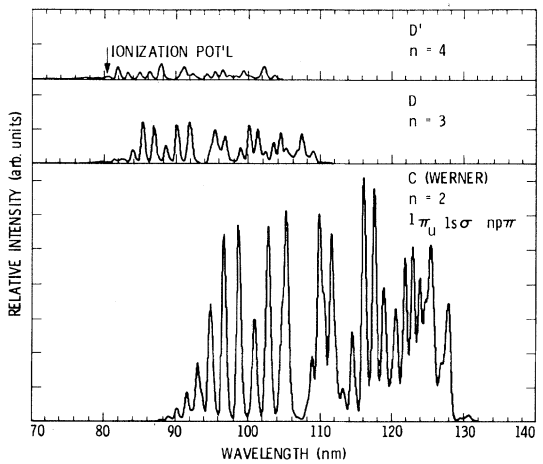

FIG. 9. A synthetic spectra of the $np\pi$ Rydberg-series emission $n=2,3,4$ where the relative intensities are normalized to our experimental values at 100 eV.

surements[5] in the 115—170-nm region, basically because the calibration factors in the present euv measurements above 115 nm are large and more uncertain. However, the cross sections estimated for the H_2 Werner system using both the euv and fuv data differ by only $\sim 15\%$, a satisfactory agreement in view of the calibration difficulties in this region (see Fig. 2). The relative cross sections of the H_2 Lyman and Werner systems are fixed largely by the fit to the data in the 120—170-nm region. The present results for the *B-X* and *C-X* cross sections are therefore based on the same data as the earlier results reported by Ajello *et al.*[5] and shown in Table II. The $\sim 25\%$ difference between the present results and the earlier work[5] (see Table II) are caused by an error in analysis in Ref. 5, rather than any basic difficulty in fitting the data. The *E,F-B* contribution to the *B*-state population was applied in a vibrational distribution fixed by a theoretical calculation in which the cubic energy factors in the transition probabilities were erroneously neglected. The consequence of this error was to produce an overestimate of the *E,F-B* contribution. A reapplication of the model calculation technique of Ref. 5 after correction of the above factors yields results within $\sim 5\%$ of the new analysis; each method uses slightly different reduction techniques.

The estimation of the *E,F-B* cascade contribution to the *B*-state population is determined mostly by fitting the model to the features in the 132-140-nm region (See Ref. 5). It has been necessary to assume a constant electronic transition moment for this system in calculating theoretical relative $g(j;v_j)$ rates for the cascade process. We have found that applying $g(j;v_j)$ values calculated in this manner can produce a satisfactory fit to the data at $E_e=100$ eV, although it is not optimal. However, at $E_e=20$ eV the cascade component is much stronger[5] and indicates a distribution in v_B substantially different from the theoretical values. In fact, at $E_e=20$ eV the *E,F-B* contribution is strong enough to obtain an experimental estimate of the relative $g(J;v_j)$, $j=B$ cascade rates, and these relative values (Table VI) have been used in establishing the cross section. The cascade process measurably affects the $v_B \leq 4$ levels. The cascade distribution estimated at $E_e=20$ eV in this manner also produces a satisfactory fit to the data at $E_e=100$ eV after appropriate adjustment of the system cross sections at the two energies. However, there is some indication that the fit at $E_e=100$ eV is still not optimal, suggesting there may be some variation in the values of g as a function of v_B for the cascade process. The experimental measurement indicates that the ratio

$$g_c(B)/g(B)\ , \tag{13}$$

where g_c is the cascade component, is very nearly constant at energies above $E_e=50$ eV, with a very sharp rise at lower energies. The present work at low energies relating to the important cascade effect is not complete, and we have only a single measurement at 20 eV. However, we have applied a theoretical analytic approximation to the *E,F-B* effective cross section using a combination of electron exchange and direct-excitation Gaunt factors[38] fitting the data points at 100 and at 20 eV, to produce an estimated cross section down to threshold (Fig. 7). The cross section peaks sharply at $E_e=17.5$ eV with a value $\sigma_c(B)=1.4\times 10^{-17}$ cm^2. Watson and Anderson[39] show direct measurements of the excitation function of selected lines of the *E,F-B* transition, and present evidence that may also indicate fairly substantial variation with E_e in $g_c(B,v_B)$ as a function of v_B. These authors[39] present results indicating measurable $H\rightarrow B$ transitions in contrast to the very low estimate by Ref. 11, and suggest that the *E* state may be populated by cascade from the *B'* state in addition to direct excitation. These are all reasons for expecting deviation of observed relative $g_c(B;v_B)$ rates as a function of v_B, but, in addition, Glass-Maujean, Dressler, and Quadrelli (private communication) have indicated that the *E,F-B* transition is affected by strong variation in the electronic transition moment. One would therefore expect deviations with calculations strictly dependent on Franck-Condon factors alone. Table VI shows the relative rates $g(j;v_j;\infty)$ used in the present calculations for all of the ground-state corrected states, normalized to a total of 1.

The observations reported here in the euv region, 70—130 nm, contain a mixture of all six band systems, but inspection of Figs. 8 and 9 show that there is sufficient separation in spectral characteristics to allow measures of each of the system cross sections, although the weaker *D'-X* and *B''-X* transitions are rather uncertain. Figure 10 shows the model fit to the data before perturbation effects were included in the calculations. Deviations assumed to be mostly due to predissociation appear principally in the 80—90-nm region and near 107 nm. Adjustments to the upper-state "radiative" populations were made iteratively to produce the model fit shown in Fig. 5. The loss and emission yields estimated in this process are shown in Table III in comparison with the work of Refs. 8 and 16 on predissociation effects. Some moderate differences appear in the Table III comparison that may be due mostly to measurement uncertainty in the present analysis. Although some levels of the *C* and *B* states show perturbation effects in high-resolution work (see Herzberg and Howe[40]), we see no evidence of consistent effects on emis-

TABLE VI. Relative excitation rates $[g(j;v_j;\infty)]$ of the H_2 Rydberg states $[\sum_{v_j} g(j;v_j;\infty)=1.0]$. Numbers in parentheses represent powers of ten, e.g., $0.600(-4)=0.600\times10^{-4}$.

v	E,F-B[a]	B-X[b]	B'-X and B''-X[c]	C-X[d]	D-X and D'-X[e]
0	0.346	0.600(−4)	0.332(−4)	0.141(−2)	0.108(−2)
1	0.242	0.203(−3)	0.737(−3)	0.211(−2)	0.182(−2)
2	0.170	0.400(−3)	0.102(−2)	0.198(−2)	0.187(−2)
3	0.144	0.602(−3)	0.114(−2)	0.153(−2)	0.154(−2)
4	0.660(−1)	0.758(−3)	0.105(−2)	0.106(−2)	0.112(−2)
5		0.861(−3)	0.674(−3)	0.700(−3)	0.772(−3)
6		0.894(−3)	0.115(−3)	0.451(−3)	0.514(−3)
7		0.874(−3)	0.210(−4)	0.287(−3)	0.338(−3)
8		0.818(−3)	0.520(−4)	0.183(−3)	0.223(−3)
9		0.736(−3)		0.117(−3)	0.148(−3)
10		0.646(−3)		0.753(−4)	0.101(−3)
11		0.557(−3)		0.479(−4)	0.690(−4)
12		0.468(−3)		0.291(−4)	0.470(−4)
13		0.391(−3)		0.138(−4)	0.330(−4)
14		0.323(−3)			0.250(−4)
15		0.265(−3)			0.700(−5)
16		0.217(−3)			
17		0.177(−3)			
18		0.143(−3)			
19		0.117(−3)			
20		0.945(−4)			
21		0.768(−4)			
22		0.625(−4)			
23		0.509(−4)			
24		0.416(−4)			
25		0.340(−4)			
26		0.279(−4)			
27		0.228(−4)			
28		0.186(−4)			
29		0.153(−4)			
30		0.126(−4)			
31		0.103(−4)			
32		0.821(−5)			
33		0.628(−5)			
34		0.445(−5)			
35		0.238(−5)			
36		0.342(−6)			

[a]Present experimental estimate of rates into v_B.
[b]Calculated from Allison and Dalgarno's data (Ref. 20).
[c]Spindler (Ref. 27) Franck-Condon factors.
[d]Spindler (Ref. 27) Franck-Condon factors.

sion rates at the resolution of this experiment. However, differences in the B-X spectrum have been observed at 156 and 161 nm and the $A(B,X;8,14)$ and $A(B,X;6,13)$ transition probabilities have been arbitrarily reduced by $\frac{1}{2}$ to fit the observations. These differences may just as easily be caused by theoretical uncertainty in the shape of the B-X continuum that underlies the discrete transitions at these locations; the shape of the potential curve near the dissociation energy is difficult to define accurately.

The model calculation of the H_2 band feature near 102.5 nm shows a deficiency relative to the data that has been attributed to the H Ly-β transition produced by dissociative excitation. The estimated cross section for the H($1s$-$3p$) Ly-β transition, 8.9×10^{-19} cm^2 (Table IV) at $E_e=100$ eV can be compared to the value derived from the measurements of Hα cross sections cited earlier in the text. The Hα (Balmer) transitions consist of the transitions $2p$-$3s$, $2p$-$3d$, and $2s$-$3p$. The volume emission rate of the Hα multiplet can thus be expressed by

$$I_{H\alpha}=F_e N_0 \sigma_{3,2}\,, \tag{14}$$

and

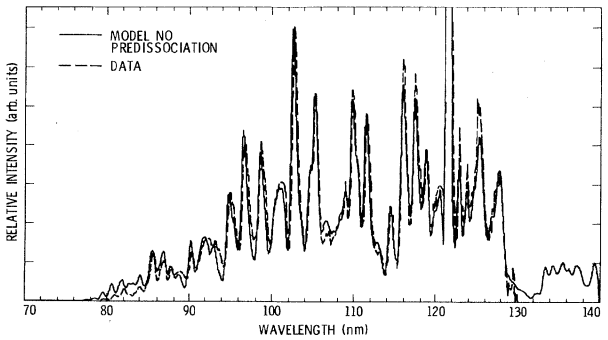

FIG. 10. Best model fit for the euv region to the laboratory spectrum of Fig. 5 with the branching yield of predissociation set equal to zero.

$$I_{H\alpha}=g_{3s}(A_{3s\,2p}/A_{3s})+g_{3p}(A_{3p\,2s}/A_{3p})$$

$$+g_{3d}(A_{3d\,2p}/A_{3d})\ . \tag{15}$$

The branching ratios are well known quantities and we have

$$A_{3s\,2p}/A_{3s}=A_{3d\,2p}/A_{3d}=1.0\ ,$$

$$A_{3p\,2s}/A_{3p}=0.119\ .$$

The relative values $g_{3s}:g_{3p}:g_{3d}$ have been measured in Ref. 31 and are in the ratio 0.057:0.54:0.41. Therefore, Eq. (15) reduces to

$$I_{H\alpha}=g_3(0.531)=F_eN_0\sigma_{3,2}\ . \tag{16}$$

The volume emission rate of H Ly-β can be written

$$I_{\text{Ly-}\beta}=F_eN_0\sigma_{3p\,1s'} \tag{17}$$

and

$$I_{\text{Ly-}\beta}=g_{3p}(A_{3p\,1s}/A_{3p})\ . \tag{18}$$

Thus

$$I_{\text{Ly-}\beta}=g_3(0.476) \tag{19}$$

and we have

$$\sigma_{3,2}/\sigma_{3p\,1s}=1.12\ , \tag{20}$$

because g_3 and F_eN_0 are in a constant ratio. If $\sigma_{3,2}=9.3\times10^{-19}$ cm^2 at $E_e=100$ eV as measured by Ref. 32 and others, then we predict

$$\sigma_{3p\,1s}=8.3\times10^{-19}\ \text{cm}^2\ ,$$

in excellent agreement with the present measurement, well within measurement uncertainty.

A comparison of the cross sections calculated in the present work with those calculated by Ref. 2 is of particular interest in relation to theoretical calculations. The experimental evidence suggests that the Gaunt[38] factors (in threshold energy units) for the excitation of the $B,B',B''\Sigma$ series and those for the C,D,D' II series show very similar shapes and magnitudes. The calculations of Ref. 2 were made by equating the Gaunt factors for the B- and C-state transitions to those for the higher members of the Σ and II series. At high electron energies the implication then was that the cross sections were in the ratios of the oscillator strengths for the transitions. Comparison with the cross sections of Ref. 2 at 100 eV suggest that the values for the B, B', B'', C, D, and D' states share the same factor of proportionality to the oscillator strengths as calculated by Miller and Krauss,[13] to within $\sim15\%$. The absolute values of Ref. 2 are roughly 15% lower than the present set of directly measured cross sections. There is rather good general agreement with the recent calculations of Arrighini *et al.*[11] (Table II) for all of the processes, with the exception of the rather low value given by Ref. 11 for direct excitation of the B state. The total C-state cross section attributed to the measurements of Stone and Zipf[15] is calculated from their measurement of the $Q(1)$ line of the (4,8) band, selected for its proximity to the 121.6-nm line in order to minimize calibration error.

The laboratory observations presented in this work now account for virtually all of the euv and fuv H_2 band emission. Further work is indicated for the E,F-B component at low energies where cascade becomes important. The higher Rydberg-series transitions, which appear measurably below 110 nm, in total have a cross section $\sim50\%$ of that of the Werner bands, and have been found essential to the interpretation of planetary euv spectra.[2] Figure 11 shows synthetic spectra indicating the relative distribution of the Lyman and Werner systems compared to the total of the B', B'', D, and D' systems. The higher series members dominate the spectrum below 90 nm. The accuracy of the model fit to the data appears to be sufficient to serve as a calibration standard for euv instruments in the 80—170-nm region, provided account is taken of optical depth effects for foreground abundance greater than 3×10^{12} cm^{-2}.

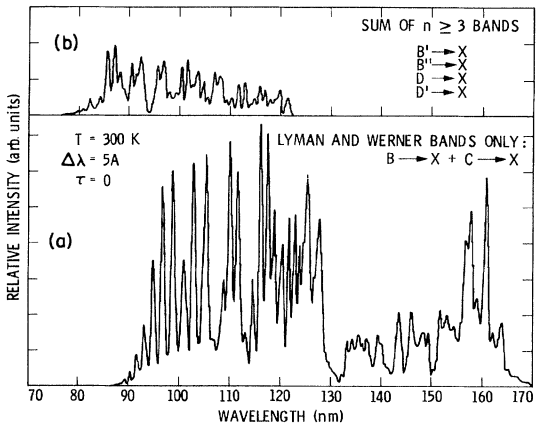

FIG. 11. (a) A theoretical model of the Lyman and Werner bands only at 0.5-nm resolution. τ is the optical depth and T is the temperature. (b) A theoretical model of the B'-X, B''-X, D-X, and D'-X band systems at 0.5-nm resolution.

One more point to discuss is a comparison of the predissociation cross section to the total dissociative cross section for production of H($n=2$) atoms. We have measured a predissociation cross section of 6.2×10^{-18} cm^2 (Table II). Mumma and Zipf[19] and Vroom and de Heer[28] have measured the total dissociative cross section for production of H(2p) of 1.2×10^{-17} cm^2 and for production of H(2s) of 6.35×10^{-18} cm^2. The sum of these two quantities yields a total dissociative cross section of 1.8×10^{-17} cm^2. The predissociation channel via the B'-state is a major source of "slow" H(1s) and metastable H(2s) atoms observed by several experimenters.[28–33,41] Based on our results we estimate that at least $\frac{1}{3}$ of all the dissociation at 100 eV lead to slow H(2s) atoms from predissociation of the D, D', and B'' states by the B' state.

CONCLUSIONS

Calibrated laboratory measurements of H_2 bands in the 70–170-nm region using crossed neutral and electron beams have allowed the estimation of the cross sections for H_2 bands which account for virtually all of the H_2 euv band emission. We find, in general, that the internal population structure of the directly excited euv band systems, B-X, B'-X, C-X, D-X, and D'-X, is modeled accurately by the theoretical collision strengths.[38] Moreover, the analysis of the measurements indicates that the same constant factor at a given electron energy at or above 100 eV, relates the theoretical oscillator strengths of the systems to the cross sections to within ~15%.

The higher-Rydberg-series band systems measured in this work have been found to be a significant factor in the analysis of euv planetary spectra. The prominence of the E,F-B contribution at low electron impact energies is also of astrophysical importance and further work is recommended to better define the excitation parameters of the E,F system.

ACKNOWLEDGMENTS

The authors thank J. A. R. Samson for interesting discussions of polarization, S. K. Srivastava for the electron-gun design, and E. C. Zipf for valuable discussions. The authors also wish to thank M. Glass-Maujean and J. Y. Roncin for valuable discussions and for communicating unpublished data. This work was supported by the U.S. Air Force Office of Scientific Research (AFOSR) Planetary Atmospheres and Astronomy/Relativity Programs of National Aeronautics and Space Administration (NASA). It represents one phase of work sponsored by NASA under Contract No. NAS7-100 to the Jet Propulsion Laboratory, California Institute of Technology, Pasadena, CA 91109. This work was also supported by NASA, Division of Planetary Sciences Grant No. NAGW-106.

[1]J. J. Hopfield, Nature 125, 927 (1930); H. Beutler, Z. Phys. Chem. B 29, 315 (1935); Y. Tanaka, Sci. Pap. Inst. Phys. Chem. Res. (Jpn.) 42, 49 (1944); A. Monfils, J. Mol. Spectrosc. 15, 205 (1965); G. Herzberg and Ch. Jungen, *ibid.* 41, 425 (1972).

[2]D. Shemansky and J. Ajello, J. Geophys. Res. 88, 459 (1983).

[3]J. M. Ajello, S. K. Srivastava, and Y. Yung, Eos 62, 940 (1981).

[4]M. Larzilliere, F. Launay, and J.-Y. Roncin, J. Phys. (Paris) 41, 1431 (1980). In addition, these authors have more work in progress covering a larger wavelength range in the euv. They clearly see several bands of the $D''\rightarrow X$ system (0-1, 0-2, 0-3, 0-4, 0-7, 0-8, 1-1, and 1-5).

[5]J. M. Ajello, S. K. Srivastava, and Y. L. Yung, Phys. Rev. A 25, 2485 (1982).

[6]K. P. Huber and G. Herzberg, *Molecular Spectra and Molecular Structure IV, Constants of Diatomic Molecules* (Van Nostrand Reinhold, New York, 1979), p. 240.

[7]P. M. Dehmer and W. A. Chupka, J. Chem. Phys. 65, 2243 (1976).

[8]P. M. Guyon, J. Breton, and M. Glass-Maujean, Chem. Phys. Lett. 68, 314 (1979); M. Glass-Maujean, J. Breton, and P. M. Guyon, *ibid.* 63, 591 (1979).

[9]A. L. Broadfoot, M. J. S. Belton, P. Z. Takacs, B. R. Sandel, D. E. Shemansky, J. B. Holberg, J. M. Ajello, S. K. Atreya, T. M. Donahue, H. W. Moos, J. L. Bertaux, J. E. Blamont, D. F. Strobel, J. C. McConnell, A. Dalgarno, R. Goody, and M. B. McElroy, Science 24, 979 (1979); A. L. Broadfoot, B. R. Sandel, D. E. Shemansky, J. B. Holberg, G. R. Smith, D. F. Strobel, J. C. McConnell, S. Kumar, D. M. Hunten, S. K. Atreya, T. M. Donahue, H. W. Moos, J. L. Bertaux, J. E. Blamont, R. B. Pomphrey, and S. Linick, *ibid.* 212, 206 (1981); A. L. Broadfoot, B. R. Sandel, D. E. Shemansky, J. C. McConnell, G. R. Smith, J. B. Holberg, S. K. Atreya, T. M. Donahue, D. F. Strobel, and J. L. Bertaux, J. Geophys. Res. 86, 8259 (1981).

[10]J. T. Clarke, H. W. Moos, S. K. Atreya, and A. L. Lane, Astrophys. J. Lett. 241, L179 (1980); Y. L. Yung, G. R. Gladstone, K. M. Chang, J. M. Ajello, and S. K. Srivastava, Astrophys. J. Lett. 254, L65 (1982).

[11]G. P. Arrighini, F. Biondi, C. Guidotti, A. Biagi, and F. Marinelli, Chem. Phys. 52, 133 (1980).

[12]L. Mu-Tao, R. Lucchese, and V. McKoy, Phys. Rev. A 26, 3240 (1982).

[13]K. J. Miller and M. Krauss, J. Chem. Phys. 47, 3754 (1967).

[14]B. R. Lewis, J. Quant. Spectrosc. Radiat. Transfer 14, 537 (1974).

[15]E. J. Stone and E. C. Zipf, J. Chem. Phys. 56, 4646 (1972).

[16]M. Rothschild, H. Egger, R. Hawkins, J. Bokor, H. Pummer, and C. Rhodes, Phys. Rev. A 23, 206 (1981).

[17]S. Takezawa, J. Chem. Phys. 52, 2575 (1970); T. Namioka, *ibid.* 41, 2141 (1964).

[18]J. M. Ajello and S. K. Srivastava, J. Chem. Phys. 75, 4454 (1981).

[19]M. J. Mumma and E. C. Zipf, J. Chem. Phys. 55, 1661 (1971).

[20]A. C. Allison and A. Dalgarno, At. Data 1, 289 (1970); A. Dalgarno, G. Herzberg, and T. L. Stephens, Astrophys. J. Lett. 162, L49 (1975).

[21]J. E. Mentall and H. D. Morgan, Phys. Rev. A 14, 954 (1976).

[22]J. Samson, *Techniques of Vacuum Ultraviolet Spectroscopy* (Wiley, New York, 1967), pp. 139 and 212.

[23]I. C. Malcolm, H. W. Dassen, and J. W. McConkey, J. Phys. B 12, 1003 (1979).

[24]J. H. Weaver, C. Krafka, D. W. Lynch, and E. E. Koch, *Physics Data—Optical Properties of Metals (Part 1)* (Fachinformations-Zentrum, Karlsruhe, Federal Republic of Germany, 1981), pp. 259—262.
[25]A. W. Fliflet and V. McKoy, Phys. Rev. A 21, 1863 (1980).
[26]D. E. Gerhardt, J. Chem. Phys. 62, 82 (1975).
[27]R. J. Spindler, J. Quant. Spectrosc. Radiat. Transfer 9, 1041 (1969); 9, 627 (1969).
[28]D. A. Vroom and F. J. de Heer, J. Chem. Phys. 50, 580 (1969).
[29]R. S. Freund, J. A. Schiovone, and D. F. Brader, J. Chem. Phys. 64, 1122 (1976).
[30]J. A. Schiovone, K. C. Smyth, and R. S. Freund, J. Chem. Phys. 63, 1043 (1975).
[31]L. Julien, M. Glass-Maujean, and J. P. Descoubes, J. Phys. B 6, L196 (1973).
[32]C. Karolis and E. Harting, J. Phys. B 11, 357 (1978).
[33]R. N. Compton and J. N. Bardsley, *Electron Molecule Collisions,* edited by K. Takayanagi (Plenum, New York, in press).
[34]B. L. Moisewitsch and S. J. Smith, *Electron Impact Excitation of Atoms,* U.S. Natl. Bur. Stand., Natl. Stand. Ref. Data Ser. NSRDS-NBS 25 (U.S. GPO, Washington, D.C. 1968), pp. 11—21.
[35]T. L. Stephens and A. Dalgarno, J. Quant. Spectrosc. Radiat. Transfer 12, 569 (1972).
[36]G. Herzberg, *Molecular Spectra and Molecular Structure I, Spectra of Diatomic Molecules* (Van Nostrand Reinhold, New York, 1950) Chaps. V—VII.
[37]M. C. Festou, S. K. Atreya, T. M. Donahue, B. R. Sandel, D. E. Shemansky, and A. L. Broadfoot, J. Geophys. Res. 86, 5715 (1981).
[38]M. J. Seaton, *Atomic and Molecular Processes,* edited by D. R. Bates (Academic, New York 1962), Chap. 11; H. S. W. Massey and E. H. S. Burhop, *Electronic and Ionic Impact Phenomena,* 2nd ed. (Clarendon, Oxford, 1969), Chap. 8.
[39]J. Watson and R. J. Anderson, J. Chem. Phys. 66, 4025 (1977).
[40]G. Herzberg and L. L. Howe, Can. J. Phys. 37, 636 (1959).
[41]S. R. Ryan, J. J. Spezeski, O. F. Kalman, W. E. Lamb, L. C. McIntyre, and W. H. Wing, Phys. Rev. A 19, 2192 (1979).